

# Comprehensive Design Space Exploration for Tensorized Neural Network Hardware Accelerators

Jinsong Zhang\*, Minghe Li\*, Jiayi Tian, Jinming Lu†, Zheng Zhang†

Department of Electrical and Computer Engineering, University of California, Santa Barbara, USA

{jinsongzhang, minghe, jiayi\_tian, jinminglu}@ucsb.edu, zhengzhang@ece.ucsb.edu

## Abstract

High-order tensor decomposition has been widely adopted to obtain compact deep neural networks for edge deployment. However, existing studies focus primarily on its algorithmic advantages—such as accuracy and compression ratio—while overlooking the hardware deployment efficiency. Such hardware-unaware designs often obscure the potential latency and energy benefits of tensorized models. Although several works attempt to reduce computational cost by optimizing the contraction sequence based on the number of multiply–accumulate operations, they typically neglect the underlying hardware characteristics, resulting in suboptimal real-world performance. We observe that the contraction path, hardware architecture, and dataflow mapping are tightly coupled and must be optimized jointly within a unified design space to maximize deployment efficiency on real devices. To this end, we propose a co-exploration framework that unifies these dimensions within a unified design space for efficient training and inference of tensorized neural networks on edge platforms. The framework formulates a latency-oriented search objective and solves it via a global latency-driven exploration across the unified design space to achieve end-to-end model efficiency. The optimized configurations are implemented on a configurable FPGA kernel, achieving up to  $4\times$  and  $3.85\times$  lower inference and training latency compared with the dense baseline.

## CCS Concepts

• Hardware → Hardware accelerators; • Computing methodologies → Modeling methodologies; Computer vision.

## Keywords

Tensor decomposition, Tensorized neural network, Hardware architecture, Design space exploration

## 1 Introduction

Deep neural networks (DNNs) have achieved remarkable success in image classification [7, 10, 19], object detection [20], and video recognition [1]. However, their rapidly growing computational and memory demands pose significant challenges for deployment on resource-constrained hardware such as FPGAs. To mitigate these limitations, a variety of model compression techniques have been proposed to reduce parameter redundancy and computational overhead, including quantization [13, 25–27], pruning [2, 3, 12, 24], and tensor decomposition [8, 9, 14, 16]. Among these methods, tensor decomposition offers an especially promising solution, achieving

orders-of-magnitude reductions in model parameters while preserving accuracy [30–32]. By representing high-dimensional weight tensors as sequences of low-rank tensor cores, tensor decomposition significantly reduces storage requirements without compromising model performance. This property enables the deployment of large-scale DNNs on lightweight edge devices, facilitating low-latency and energy-efficient real-world applications.

Although tensorized neural networks (TNNs) have demonstrated ultra-low model sizes, prior algorithm-level designs often overlook the actual hardware efficiency, thereby failing to achieve true acceleration and energy benefits in real deployments.

Recent studies have shown that the contraction sequence can greatly impact the computational cost of TNNs. Gu et al. [5] partially addressed this issue by searching for contraction paths that minimize the number of multiply–accumulate (MAC) operations, while Tian et al. [22] adopted a fixed bi-directional contraction path to enhance intra-sequence parallelism. These approaches mainly focus on reducing theoretical MAC, without considering real-time execution latency. More recently, Zhang et al. [33] introduced a mapping-aware contraction sequence search algorithm that incorporates hardware considerations into sequence optimization. However, their design supports only sequential contraction paths starting from the input node, whose search space ignores both the intra-sequence parallelism inherent in tensorized structures and the tensor-core-primary contraction order, thereby often leading to suboptimal paths.

To overcome these limitations, we propose a comprehensive design space exploration (DSE) and architecture generation framework that optimizes jointly the contraction paths, hardware architecture, and dataflow for end-to-end TNN training and inference on edge devices.

We first formulate a latency-oriented configuration search objective to identify the optimal combination of design parameters that minimize overall execution latency. To improve search efficiency, the contraction path search space is constrained by a MAC-guided sequence exploration algorithm, which prunes redundant high-cost paths while preserving promising low-MAC candidates. Next, we simulate the latency of all feasible configuration combinations within the unified search space and employ a global latency-driven search algorithm to select the model-level optimal configuration. Through this comprehensive DSE framework, our approach surpasses prior local (layer-wise) search methods, achieving superior end-to-end hardware efficiency and overall model speedup. Finally, to validate the effectiveness of our framework, we deploy the optimized designs on an FPGA platform and evaluate their actual runtime performance.

**Paper Contributions.** Our contributions could be summarized as the following:

\*Equal contribution. Listed in alphabetical order.

†Corresponding author.

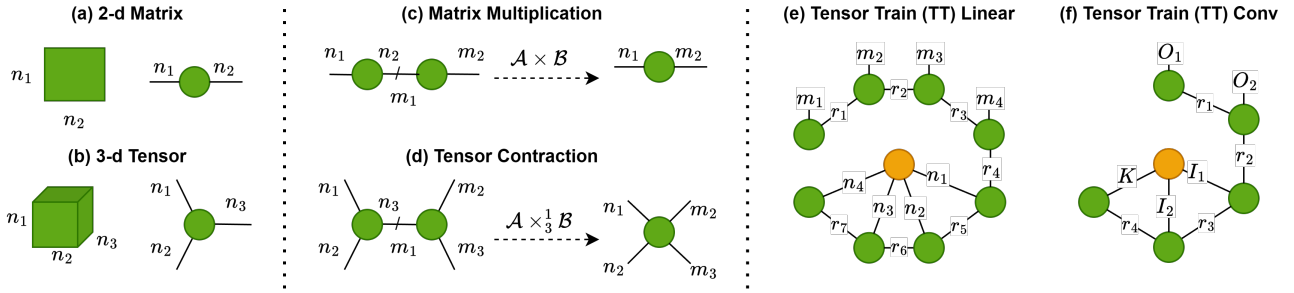


Figure 1: Tensor graph representations of (a) matrix, (b) tensor, (c) matrix multiplication, (d) tensor contraction, (e) tensor train (TT) format linear layer, and (f) tensor train (TT) format convolution layer.

- We propose a comprehensive design space exploration framework that jointly explores contraction paths, hardware architectures, and dataflow to minimize end-to-end latency for tensorized neural networks (TNNs) on edge devices.
- We develop a global latency-driven search algorithm that efficiently evaluates and selects configuration combinations across layers and hardware settings from a whole-model perspective.
- We design a parameterized GEMM kernel on FPGA and validate the optimized design through real-world implementation, demonstrating significant improvements in latency and hardware efficiency.

## 2 Background

### 2.1 Tensor Basics

**Tensor** is a high-dimensional data structure [11], and a tensor with  $d$  dimensions (or modes) could be represented as  $\mathcal{A} \in \mathbb{R}^{n_1 \times \dots \times n_d}$ , where  $n_k$  is the size of mode  $k$ . For clarity, tensor operations can also be visualized using graph representations. As illustrated in Fig. 1 (a)-(b), a  $d$ -way tensor is represented by a node with  $d$  edges, where a matrix corresponds to a 2-way tensor.

**Tensor contraction** refers to the operation that multiplies two tensors along a shared mode, effectively eliminating that mode and producing a new tensor. Consider tensors  $\mathcal{A} \in \mathbb{R}^{n_1 \times \dots \times n_d}$  and  $\mathcal{B} \in \mathbb{R}^{m_1 \times \dots \times m_d}$ .

We use  $\times_s^t$  to denote the contraction between the  $s$ -th mode of  $\mathcal{A}$  and the  $t$ -th mode of  $\mathcal{B}$ , where the dimensions match ( $n_s = m_t$ ). The resulting tensor can be written as

$$C = \mathcal{A} \times_s^t \mathcal{B}, \quad \text{where } C \in \mathbb{R}^{\prod_{i \neq s}^{d-1} n_i \times \prod_{j \neq t}^{d-1} m_j}. \quad (1)$$

Fig. 1(c) and (d) illustrate examples of tensor contractions between 2-way and 3-way tensors, where the former is equivalent to standard matrix multiplication. The number of remaining (unconnected) edges—often referred to as free edges—determines the order and dimensionality of the resulting tensor.

### 2.2 Tensorized Neural Network

Tensor decomposition has been used to compress neural networks, among which tensor train (TT) decomposition [17] is particularly popular due to their high reconstruction accuracy, orders-of-magnitude compression ratios, and low computational overhead [16, 28, 29]. In

the following, we describe how a weight matrix can be factorized into multiple smaller tensor cores using TT decompositions.

**Tensorized Linear Layer.** Consider a weight matrix  $\mathbf{W} \in \mathbb{R}^{M \times N}$  in a linear layer. Assuming  $M = \prod_i^d m_i$  and  $N = \prod_i^d n_i$ , we first reshape  $\mathbf{W}$  into a  $2d$ -way tensor  $\mathcal{W} \in \mathbb{R}^{m_1 \times \dots \times m_d \times n_1 \times \dots \times n_d}$ . With TT decomposition, we can represent  $\mathcal{W}$  with TT cores  $\{\mathcal{G}_k\}_{k=1}^{2d}$  as

$$\mathcal{W} = \mathcal{G}_1 \times_3^1 \dots \mathcal{G}_k \times_3^1 \dots \mathcal{G}_d \times_3^1 \dots \mathcal{G}_{d+k} \times_3^1 \mathcal{G}_{2d}. \quad (2)$$

Here  $\mathcal{G}_k \in \mathbb{R}^{r_{k-1} \times m_k \times r_k}$  when  $1 \leq k \leq d$  and  $\mathcal{G}_k \in \mathbb{R}^{r_{k-1} \times n_{k-d} \times r_k}$  when  $d+1 \leq k \leq 2d$ . In TT decomposition, the boundary ranks satisfy  $r_0 = r_{2d} = 1$ . The number of parameters in  $\mathcal{W}$  approximately achieves  $O(m^d n^d) \rightarrow O(dr^2(m+n))$  memory reduction. In this way, the forward propagation of a tensorized linear layer could be represented as

$$\mathcal{Y}[i_1, \dots, i_d] = \mathcal{G}_1[i_1] \dots \mathcal{G}_d[i_d] \sum_{j_1, \dots, j_d}^{n_1, \dots, n_d} \mathcal{G}_{d+1}[j_1] \dots \mathcal{G}_{2d}[j_d] \mathcal{X}[j_1, \dots, j_d],$$

where the input tensor  $\mathcal{X} \in \mathbb{R}^{n_1 \times \dots \times n_d}$ , and the resulted output  $\mathcal{Y} \in \mathbb{R}^{m_1 \times \dots \times m_d}$ . Figure 1(e) illustrates the tensor-graph representations of TT-format linear layer. As shown, the tensor cores are connected via rank dimensions, while the input tensor interacts with multiple cores through the corresponding input modes. The free edges in the network correspond to the output feature dimensions.

**Tensorized Convolution Layer.** For a standard 2D convolutional layer with kernel  $\mathcal{W} \in \mathbb{R}^{C_{out} \times C_{in} \times K_h \times K_w}$ , we decompose the channel dimensions ( $C_{out} = O_1 \times O_2$ ,  $C_{in} = I_1 \times I_2$ ) and merge spatial dimensions into  $K = K_h K_w$ . Using TT decomposition,  $\mathcal{W}$  is factorized into a sequence of five cores  $\{\mathcal{G}_k\}_{k=1}^5$ :

$$\mathcal{W} = \mathcal{G}_1 \times_3^1 \mathcal{G}_2 \times_3^1 \mathcal{G}_3 \times_3^1 \mathcal{G}_4 \times_3^1 \mathcal{G}_5. \quad (3)$$

Here, the cores are defined as  $\mathcal{G}_1 \in \mathbb{R}^{1 \times O_1 \times r_1}$ ,  $\mathcal{G}_2 \in \mathbb{R}^{r_1 \times O_2 \times r_2}$  (encoding output channels),  $\mathcal{G}_3 \in \mathbb{R}^{r_2 \times I_1 \times r_3}$ ,  $\mathcal{G}_4 \in \mathbb{R}^{r_3 \times I_2 \times r_4}$  (encoding input channels), and  $\mathcal{G}_5 \in \mathbb{R}^{r_4 \times K \times 1}$  (spatial kernel). This reduces parameter complexity from  $O(C_{out} C_{in} K)$  to  $O(r^2(C_{out} + C_{in}) + rK)$ .

The forward propagation is performed on the unfolded input tensor  $\mathcal{X}_{unf} \in \mathbb{R}^{I_1 \times I_2 \times K \times L}$  (where  $L$  is spatial patches). The output feature map  $\mathcal{Y}_{col}$  is computed as:

$$\mathcal{Y}_{col}[o_1, o_2] = \underbrace{\mathcal{G}_1[o_1] \mathcal{G}_2[o_2]}_{\text{Output Cores}} \sum_{i_1, i_2, k} \underbrace{\mathcal{G}_3[i_1] \mathcal{G}_4[i_2] \mathcal{G}_5[k]}_{\text{Input Cores}} \mathcal{X}_{unf}[i_1, i_2, k]. \quad (4)$$

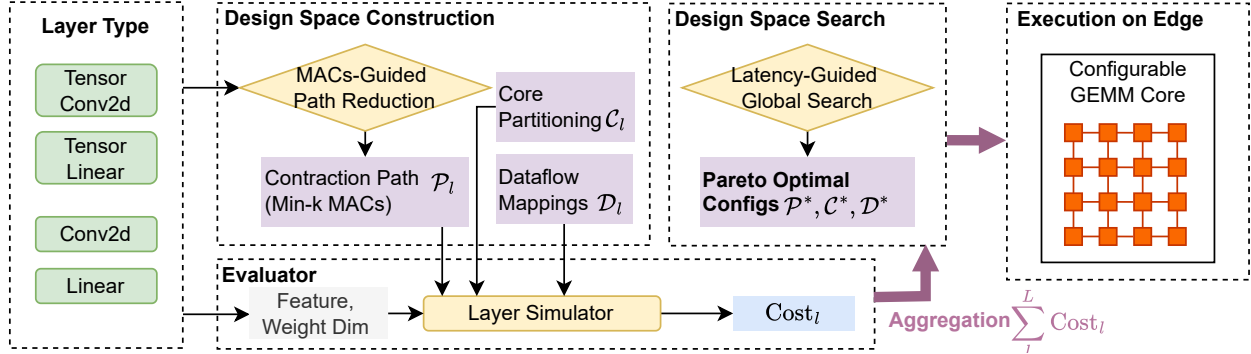


**Figure 2: Overview of the proposed DSE framework.** We first construct the layer-wise design space comprising contraction paths  $\mathcal{P}_l$ , core partitioning options  $\mathcal{C}_l$ , and dataflow mappings  $\mathcal{D}_l$ . Next, we simulate the costs of all feasible configuration combinations for each layer. Finally, a global search identifies the Pareto-optimal  $(\mathcal{P}^*, \mathcal{C}^*, \mathcal{D}^*)$  configuration that minimizes the overall model execution cost for efficient edge deployment.

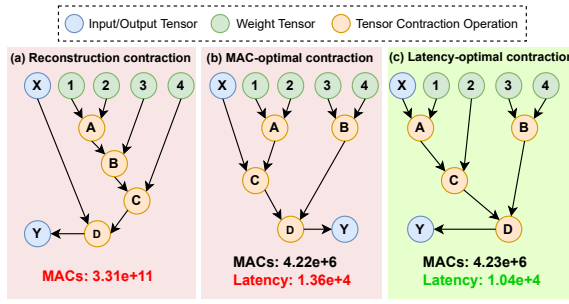


**Figure 3: The MACs and latency of different contraction sequences for a tensorized layer.** Left: reconstruction-based contraction sequence; Middle: MAC-optimal contraction sequence; Right: latency-optimal contraction sequence.

As shown in Fig. 1(f), the input tensor interacts primarily with  $\mathcal{G}_3, \mathcal{G}_4, \mathcal{G}_5$ , while the final output dimensions are generated by  $\mathcal{G}_1$  and  $\mathcal{G}_2$ .

### 3 Design Space Exploration Framework

As discussed in the introduction, different contraction paths in a TNN lead to substantially different computational costs, while hardware configurations and dataflow strategies further affect latency and utilization efficiency. To identify the most hardware-efficient combination, we develop a cost-optimal design space exploration framework that jointly considers contraction paths, core partitioning, and dataflow mappings for TNN deployment. The remainder of this section presents the problem formulation, the construction of the design spaces, and our cost-guided search algorithm for selecting the optimal configuration.

#### 3.1 Problem Formulation and Overview

Given a TNN with weights represented in TT format, let  $\mathcal{P}_l$  denote the set of candidate contraction paths for the  $l$ -th layer,  $\mathcal{D}_l$  the dataflow mapping space, and  $\mathcal{H}$  the set of global hardware

partitioning strategies, where each strategy  $h \in \mathcal{H}$  defines a valid subset of core partitioning configurations  $\mathcal{C}_h$ . For the entire model, we define the configuration sets  $\mathcal{P} = \{\mathcal{P}_l\}_{l=1}^L, \mathcal{C} = \{\mathcal{C}_l\}_{l=1}^L, \mathcal{D} = \{\mathcal{D}_l\}_{l=1}^L$ . Our objective is to determine the Pareto-optimal configuration  $(h^*, \mathcal{P}^*, \mathcal{C}^*, \mathcal{D}^*)$  by minimizing the end-to-end execution cost across all layers:

$$(h^*, \mathcal{P}^*, \mathcal{C}^*, \mathcal{D}^*) = \underset{\substack{h \in \mathcal{H}, \\ \{\mathcal{P}_l, \mathcal{C}_l, \mathcal{D}_l\}_{l=1}^L}}{\operatorname{argmin}} \left( \sum_{l=1}^L \operatorname{Cost}(\mathcal{P}_l, \mathcal{C}_l, \mathcal{D}_l) \right) \quad (5)$$

$$\text{s.t. } p_l \in \mathcal{P}_l, \quad d_l \in \mathcal{D}_l, \quad c_l \in \mathcal{C}_h$$

which yields the layer-wise optimal selections that jointly minimize the global execution cost for the full model under the optimal hardware strategy constraint.

As shown in Figure 2, our DSE framework consists of three stages: (1) design space construction for contraction paths, core partitioning strategies, and dataflow mappings; (2) layer-wise cost evaluation using a simulator; and (3) global cost aggregation and search to identify the Pareto-optimal configuration set for full-model deployment.

#### 3.2 Design Space Construction

To manage the combinatorial explosion of tensor contraction orders, we perform a MAC-guided Depth-First Search (DFS) to search for the top- $K$  paths with the lowest MACs, forming the candidate set  $\mathcal{P}_l$ . To ensure candidate diversity, we develop a redundancy-pruning strategy integrated into the recursive search, which efficiently eliminates computationally equivalent paths and prunes prohibitively expensive branches. This yields a final contraction-path space  $\mathcal{P}_l = \{p_0, p_1, \dots, p_K\}$ , consisting of the  $K$  lowest-MAC paths.

Besides the contraction path search space  $\mathcal{P}_l$ , we construct the core partitioning space and dataflow mapping space  $\mathcal{D}_l$ . As shown in [22], many tensor contractions within a TT layer are independent and can be executed in parallel. To exploit this inherent intra-layer parallelism for better latency-utilization trade-off, we introduce the global strategy space  $\mathcal{H}$  to constrain the partitioning configurations.

**Algorithm 1** Global Latency-Driven DSE Framework

**Input:** TNN Model  $\mathcal{M}$  ( $L$  layers); Global Strategy Space  $\mathcal{H}$  (where  $h \in \mathcal{H}$  constrains  $C$  to  $C_h$ ); Dataflow Space  $\mathcal{D}$ .  
**Output:** Optimal Strategy  $h^*$  and Parameters  $(\mathcal{P}^*, \mathcal{C}^*, \mathcal{D}^*)$ .

**Step 1: Design Space Construction & Cost Initialization**

- 1: Obtain  $\mathcal{P}_l$  via  $\text{FindTopK\_MAC\_Paths}(\mathcal{M}_l)$  for all layers.
- 2: Populate Cost Table  $\mathcal{T}[l, p, c, d] \leftarrow \text{Simulate}(p, c, d)$  for all valid configs.

**Step 2: Global Optimization**

- 3:  $Cost_{min} \leftarrow \infty$ ; Initialize  $(\mathcal{P}^*, \mathcal{C}^*, \mathcal{D}^*) \leftarrow \emptyset$
- 4: **for all**  $h \in \mathcal{H}$  **do** ▷ Iterate Global Core Partitioning Strategies
- 5:     Minimize layer-wise latency under hardware constraint  $C_h$
- 6:      $Cost_h \leftarrow \sum_{l=1}^L \left( \min_{p \in \mathcal{P}_l, c \in C_h, d \in \mathcal{D}} \mathcal{T}[l, p, c, d] \right)$
- 7:     **if**  $Cost_h < Cost_{min}$  **then**
- 8:          $Cost_{min} \leftarrow Cost_h$ ;  $h^* \leftarrow h$
- 9:         Update  $(\mathcal{P}^*, \mathcal{C}^*, \mathcal{D}^*)$  with the arguments from the min operation.
- 10:      **end if**
- 11:     **end for**
- 12: **return**  $(h^*, \mathcal{P}^*, \mathcal{C}^*, \mathcal{D}^*)$

For instance, a monolithic strategy restricts layers to use the full array (i.e.,  $C_h = \{1 \times 1\}$ ), while a split strategy enables sub-core parallelism (e.g.,  $C_h = \{1 \times 2, 2 \times 1\}$ ), allowing strictly vertical or horizontal partitioning of the PE array. The dataflow mapping space is defined as  $\mathcal{D}_l = \{IS, OS, WS\}$  representing the systolic-array data reuse strategies of input-stationary, output-stationary, and weight-stationary mappings.

### 3.3 Design Space Search

To efficiently navigate the design space, we propose a three-phase exploration framework as outlined in Algorithm 1. First, we reduce the search space by identifying the Top- $K$  computation paths for each layer  $l$  (denoted as  $\mathcal{P}_l$ ) based on MAC utilization. Following this pruning, we evaluate the execution cost using a simulator [18]. We populate a cost set  $\mathcal{T}$ , where  $\mathcal{T}[l, p, c, d]$  denotes the latency for each valid combination of path  $p \in \mathcal{P}_l$ , partitioning  $c \in C_{all}$ , and dataflow  $d \in \mathcal{D}$ .

Finally, we formulate the global optimization problem as a hierarchical search. Since the choice of global strategy  $h$  constrains the available partitioning options, we first iterate through each strategy  $h \in \mathcal{H}$ . Under a fixed strategy, the problem decomposes into independent layer-wise sub-problems, where we minimize the latency for each layer  $l$  within the constrained space  $C_h$  to identify the globally optimal strategy  $h^*$  and parameters  $(\mathcal{P}^*, \mathcal{C}^*, \mathcal{D}^*)$ . This methodology effectively avoids brute-force iteration, mathematically guaranteeing the optimal solution with minimal overhead.

Figure 3 validates our DSE on a tensorized ViT-Ti/4 layer (CIFAR-10) under fixed hardware constraints. By exploring the full partitioning and dataflow space, we observe that the theoretical MAC-optimal path often fails to minimize execution time due to hardware inefficiencies. In contrast, our framework identifies a latency-optimal configuration that reduces latency by 25% compared to the MAC-optimal baseline, despite a slightly higher operation count.

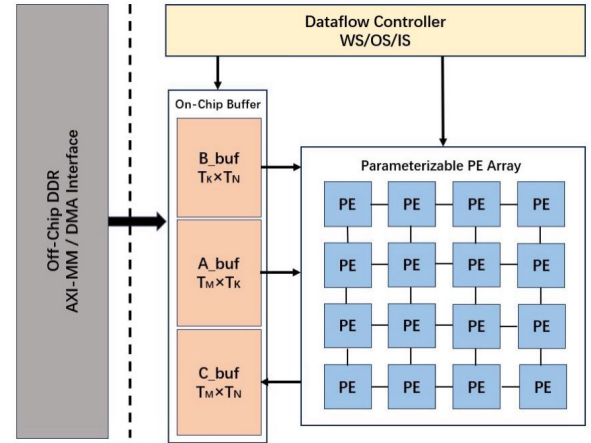


**Figure 4: Parameterizable  $M_{PE} \times N_{PE}$  systolic-style array with shared on-chip memory hierarchy.**

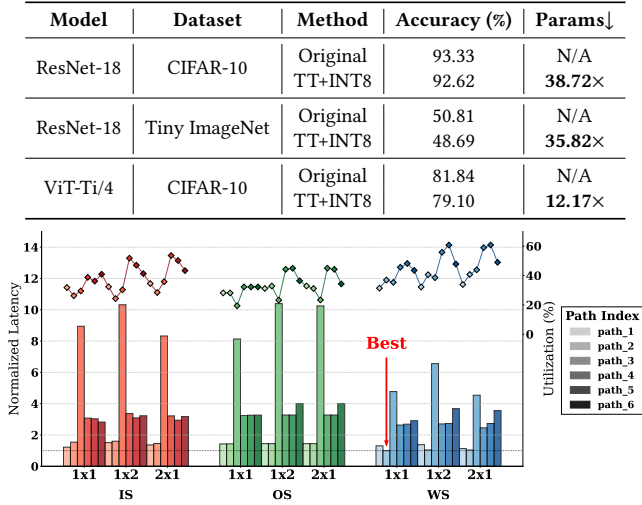
## 4 Hardware Architecture Design

We develop a parameterizable compute engine to execute tensorized layers, constructed according to the optimal configuration decisions produced by the DSE framework. The accelerator consists of two tightly coupled components: (i) a parameterizable systolic GEMM engine with flexible dataflow mappings, and (ii) a fully streaming TT contraction kernel that adapts to the heterogeneous matrix shapes induced by TT decomposition. Together, these components form a unified accelerator to execute efficient TNN training and inference with high utilization and low latency across various benchmarks.

### 4.1 Systolic GEMM Engine

Figure 4 illustrates the systolic-style compute core and its memory hierarchy. We employ a configurable  $M_{PE} \times N_{PE}$  systolic array, coupled with a tiling-based memory subsystem to handle the highly irregular matrix shapes ( $M, K, N$ ) arising from TT contractions. This subsystem decouples the problem dimensions from the fixed hardware by decomposing the computation into smaller tiles  $\langle T_M, T_N, T_K \rangle$ , thereby enabling efficient execution.

**Dataflow Flexibility (WS/OS/IS).** To sustain high utilization and low latency for various feature and weight dimensions in multiple models and datasets, and to support efficient training and inference under the irregular shapes produced by TT contractions, the GEMM engine supports three classical dataflows: weight-stationary (WS), output-stationary (OS), and input-stationary (IS). Each mapping strategically reuses different operands within the systolic array. This minimizes on-chip traffic for a given contraction shape, which in turn eliminates data starvation and maximizes hardware utilization across diverse workload characteristics. The DSE framework selects layer-wise dataflow mappings that collectively minimize the end-to-end execution cost. The switch between dataflows is realized through the dynamic reconfiguration of three hardware primitives: the multiplexer networks governing data paths, the logical roles of on-chip buffers, and the stationary operand selection within each PE's control registers. This enables seamless transitions with minimal overhead.

**Table 1: Comparison between quantized tensorized model and original model across multiple benchmarks.****Figure 5: Latency comparison across Top-K contraction paths, different dataflow mappings, and core partitioning.**

## 4.2 Streaming TT Contraction Kernel

A tensorized layer forward / backward could be decomposed into a sequence of GEMM-based contractions, whose matrix shapes are governed by the TT ranks, tensor core dimensions, and the contraction path. These contractions often exhibit heterogeneous dimensions and may include naturally intra-layer parallelism. Our contraction kernel is designed to leverage both streaming data reuse and fine-grained intra-layer parallelism through a multi-core execution fabric.

**Multi-Core Parallel Contraction.** To exploit intra-layer parallelism, the kernel employs a dual-core systolic subsystem with two identical  $M_{PE} \times \frac{N_{PE}}{2}$  or  $\frac{M_{PE}}{2} \times N_{PE}$  PE arrays. When a TT layer yields two independent contraction branches, the two arrays process them concurrently. Once these parallelizable contractions complete, both cores are reassigned to jointly execute the subsequent dependent contractions sequentially. This dual-core approach enables intra-layer parallelism with hardware reuse and preserves inter-stage data dependencies.

**Unified Execution Across All TT Contraction Paths** By integrating streaming execution, multi-core parallelism, and flexible dataflow mappings, the TT contraction kernel efficiently supports diverse input dimensions, benchmarks, and both training and inference workloads within a unified reconfigurable architecture. This design avoids the need for per-layer hardware specialization, maximizes on-chip data reuse, and provides a scalable execution framework for deploying TT- linear and convolution layers

## 5 Experimental Results

### 5.1 Experimental Setup

**Benchmarks.** To evaluate the effectiveness of our design space exploration framework, we perform experiments across a diverse

**Table 2: Distribution of layer-wise optimal configuration choices identified by our DSE framework.**

Model	Mode	Core $C^*$ (S / M)	Path $\mathcal{P}^*$ (Path-1 / k)	Dataflow $\mathcal{D}^*$ (IS / OS / WS)
ResNet-18 on Tiny ImageNet	Inference	0% / 100%	75% / 25%	50% / 50% / 0%
	Training	0% / 100%	75% / 25%	62.5% / 37.5% / 0%
ResNet-18 on CIFAR-10	Inference	0% / 100%	75% / 25%	25% / 75% / 0%
	Training	0% / 100%	75% / 25%	43.8% / 56.2% / 0%
ViT-Ti/4 on CIFAR-10	Inference	50% / 50%	50% / 50%	0% / 0% / 100%
	Training	50% / 50%	50% / 50%	0% / 66.6% / 33.3%

**Table 3: Comparison of FPGA resource utilization, power consumption, and execution latency for inference and training over multiple benchmarks.**

Benchmark	Method	BRAM	FF	LUT	Power (W)	Latency (ms)
<b>Inference</b>						
ResNet-18 on Cifar-10	Org. TT-opt	892	342k	318k	14.2	6.40
		956	408k	390k	<b>11.8</b>	<b>1.60 (4.00×)</b>
ResNet-18 on Tiny ImageNet	Org. TT-opt	1125	415k	388k	15.8	19.20
		922	475k	452k	<b>12.5</b>	<b>4.90 (3.92×)</b>
ViT-Ti/4 on Cifar-10	Org. TT-opt	1085	368k	345k	15.1	8.69
		1010	422k	396k	<b>12.7</b>	<b>2.65 (3.28×)</b>
<b>Training</b>						
ResNet-18 on Cifar-10	Org. TT-opt	1580	452k	428k	25.8	20.4
		1482	524k	525k	<b>21.2</b>	<b>5.30 (3.85×)</b>
ResNet-18 on Tiny ImageNet	Org. TT-opt	1725	540k	510k	26.1	61.5
		1428	595k	565k	<b>22.8</b>	<b>16.1 (3.82×)</b>
ViT-Ti/4 on Cifar-10	Org. TT-opt	1620	481k	458k	26.7	24.3
		1515	531k	534k	<b>22.5</b>	<b>7.11 (3.42×)</b>

set of models and tasks. Table 1 summarizes the performance of these benchmark models and datasets, detailing both accuracy and compression ratios obtained using quantized TNNs in end-to-end training. The results show that quantized TNN training achieves accuracy comparable to full-precision uncompressed models while reducing the number of model parameters by  $12 \sim 39\times$ . This substantial reduction greatly improves the feasibility of on-device training by lowering both memory footprint and computational cost.

**Simulator Settings.** We evaluate performance using a systolic array simulator configured with a  $32 \times 32$  PE array. The system includes 3072 KB SRAM for inputs and filters, 1024 KB for outputs, and a bandwidth of 256. To optimize efficiency, our framework explores variable core partitioning configurations ( $1 \times 1, 2 \times 1, 1 \times 2$ ) and searches dataflows between IS, WS, and OS. **FPGA Implementation.** After determining the optimal hardware configurations and contraction paths, we map them onto an FPGA platform to evaluate real-world execution latency and energy consumption. We develop the configurable GEMM kernel in C++ using high-level synthesis (HLS), and perform synthesis, placement, and routing using Vitis HLS 2024.2 targeting a Xilinx Virtex UltraScale+ VU9P

**Table 4: Comparison with prior FPGA CNN training accelerators.**

Attribute	[4]	[23]	[21]	[15]	[13]	[6]	Ours
Model	VGG16	ResNet-20	VGG16	VGG-like	VC709	ResNet-20	<b>ResNet-18</b>
Dataset	CIFAR-10	CIFAR-10	ImageNet	CIFAR-10	CIFAR-10	CIFAR-10 & SVHN	<b>CIFAR-10</b>
BRAM	1045	2558	812	1232	240	1735	<b>1482</b>
DSP	1037	1040	1680	6241	1728	502	<b>1024</b>
Eff.(GOPS/W)	N/A	9	8.2	0.82	4.5	15.1	<b>19.19</b>
Device	ZCU111	Stratix 10 MX	ZCU102	MAX5	VC709	ZCU102	<b>VU9P</b>
Precision	INT8	FP16	FP32	INT8	PINT8	bm(2,5)	<b>INT8</b>

FPGA. All model parameters, activations, and gradients used during both training and inference are quantized to INT8, and the design is evaluated at a 200-MHz frequency.

## 5.2 Design Space Exploration Results

**5.2.1 Layer-level Comparison.** Figure 5 further illustrates this latency variation. Even for the same tensor contraction path, different dataflow mappings (IS, OS, WS) and core partitions (eg.  $1 \times 2$  corresponds to using two  $32 \times 16$  cores) result in significantly different latency outcomes. For instance, the Weight Stationary (WS) dataflow demonstrates superior performance in specific layers, highlighting the necessity of our **joint DSE framework** that co-optimizes the contraction path, hardware architecture, and dataflow mapping simultaneously.

**5.2.2 Model-level Comparison.** Table 2 compares the theoretically minimal MAC path (**Path-1**) against the latency-optimized path (**Path-k**) identified by our framework. Notably, the framework selects the non-MAC-optimal Path-k in 25% of ResNet-18 cases and 50% of ViT-Ti inference scenarios, confirming that **MAC-only optimization is insufficient**. Regarding dataflow, our global search adapts configurations per layer: ResNet-18 favors IS over OS during training while avoiding WS globally; conversely, ViT inference uniformly adopts WS, whereas training utilizes OS more frequently. Crucially, these results demonstrate that the contraction path with the lowest theoretical cost does not guarantee the lowest hardware latency, which depends heavily on the interplay between contraction paths, hardware partitioning, and dataflow strategies.

## 5.3 FPGA Performance

**5.3.1 System-Level Efficiency and Performance.** We evaluate the end-to-end performance and efficiency of our design across three representative workloads: (1) ResNet-18 on CIFAR-10, (2) ResNet-18 on Tiny ImageNet, and (3) ViT-Ti/4 on CIFAR-10. As summarized in Table 3, which compares FPGA resource utilization, power consumption, and execution latency, our TT-optimized design delivers substantial improvements.

The optimized design achieves a latency speedup of **3.28×–4.00×** for inference and **3.42×–3.85×** for training across all benchmarks. This performance gain stems from a favorable resource-performance trade-off: while the augmented contraction-control logic introduces a modest increase in FF/LUT usage, it enables a

significant reduction in BRAM requirements (by up to **18%** in training). The net system power is reduced by **16.9–20.9%** for inference and **17.8–21.0%** for training, confirming that the energy saved from reduced data movement decisively outweighs the control overhead. These results collectively confirm that our TT-based optimization consistently enhances computational efficiency and reduces energy consumption across both CNN and ViT models in inference and training scenarios.

**5.3.2 Comparison with Previous Works.** Table 4 compares our end-to-end ResNet-18 performance with representative FPGA CNN training accelerators. To enable a fair and meaningful cross-work comparison, we adopt ResNet-18 on CIFAR-10 as the canonical benchmark, since existing FPGA accelerators rarely report results on Tiny ImageNet or ViT-style architectures, making direct apples-to-apples comparisons on these workloads infeasible. Within this widely used evaluation setting, our design achieves a peak energy efficiency of **19.19 GOPS/W** in INT8 precision on the VU9P device, delivering **1.27×** and **2.13×** higher efficiency than [6] and [23], respectively, while maintaining moderate BRAM (1482) and DSP (1024) usage. These results demonstrate the strong balance of efficiency and resource utilization achieved by our architecture, and additional experiments on Tiny ImageNet and ViT further validate its scalability across more challenging workloads.

## 6 Conclusion

In this paper, we proposed a comprehensive design space exploration (DSE) and hardware generation framework for executing efficient tensorized neural networks (TNNs) on edge devices. Our framework unifies contraction path search, core partitioning, and dataflow mapping into a global latency-driven optimization. This unified approach enables the framework to deliver optimal latency by automatically selecting a unique configuration for each model. We further realize the searched configurations on a parameterizable FPGA accelerator with a streaming TT contraction kernel that supports all tensorized layers using a single bitstream. Across ResNet-18 (CIFAR-10 / Tiny ImageNet) and ViT-Ti/4 (CIFAR-10), this co-designed system achieves **3.28×–4.00×** lower inference latency and **3.42×–3.85×** lower training latency than the dense baselines, while reducing power consumption by **17.8%–21.0%**. These consistent gains on both CNN and ViT workloads demonstrate the effectiveness of our framework in bridging algorithmic tensorization and practical hardware efficiency.

## References

- [1] Yin Fan, Xiangju Lu, Dian Li, and Yuanliu Liu. 2016. Video-based emotion recognition using CNN-RNN and C3D hybrid networks. In *Proceedings of the 18th ACM international conference on multimodal interaction*. 445–450.
- [2] Chao Fang, Wei Sun, Aojun Zhou, and Zhongfeng Wang. 2023. CEST: Computation-efficient N: M sparse training for deep neural networks. In *2023 Design, Automation & Test in Europe Conference & Exhibition (DATE)*. IEEE, 1–2.
- [3] Chao Fang, Wei Sun, Aojun Zhou, and Zhongfeng Wang. 2023. Efficient n: m sparse dnn training using algorithm, architecture, and dataflow co-design. *IEEE Transactions on Computer-Aided Design of Integrated Circuits and Systems* 43, 2 (2023), 506–519.
- [4] Sean Fox, Julian Faraone, David Boland, Kees Vissers, and Philip HW Leong. 2019. Training deep neural networks in low-precision with high accuracy using FPGAs. In *2019 International Conference on Field-Programmable Technology (ICFPT)*. IEEE, 1–9.
- [5] Jiaqi Gu, Ben Keller, Jean Kossaifi, Anima Anandkumar, Brucek Khailany, and David Z Pan. 2022. Heat: Hardware-efficient automatic tensor decomposition for transformer compression. *arXiv preprint arXiv:2211.16749* (2022).
- [6] Chuliang Guo, Binglei Lou, Xueyuan Liu, David Boland, Philip HW Leong, and Cheng Zhuo. 2023. BOOST: Block minifloat-based on-device CNN training accelerator with transfer learning. In *2023 IEEE/ACM International Conference on Computer Aided Design (ICCAD)*. IEEE, 1–9.
- [7] Tianmei Guo, Jiwen Dong, Henjian Li, and Yunxing Gao. 2017. Simple convolutional neural network on image classification. In *2017 IEEE 2nd International conference on big data analysis (ICBDA)*. IEEE, 721–724.
- [8] Cole Hawkins, Xing Liu, and Zheng Zhang. 2022. Towards compact neural networks via end-to-end training: A Bayesian tensor approach with automatic rank determination. *SIAM Journal on Mathematics of Data Science* 4, 1 (2022), 46–71.
- [9] Cole Hawkins and Zheng Zhang. 2021. Bayesian tensorized neural networks with automatic rank selection. *Neurocomputing* 453 (2021), 172–180.
- [10] Kaiming He, Xiangyu Zhang, Shaoqing Ren, and Jian Sun. 2016. Deep residual learning for image recognition. In *Proceedings of the IEEE conference on computer vision and pattern recognition*. 770–778.
- [11] Tamara G Kolda and Brett W Bader. 2009. Tensor decompositions and applications. *SIAM review* 51, 3 (2009), 455–500.
- [12] Jimming Lu, Jian Huang, and Zhongfeng Wang. 2022. THETA: A high-efficiency training accelerator for DNNs with triple-side sparsity exploration. *IEEE Transactions on Very Large Scale Integration (VLSI) Systems* 30, 8 (2022), 1034–1046.
- [13] Jimming Lu, Chao Ni, and Zhongfeng Wang. 2022. ETA: An efficient training accelerator for DNNs based on hardware-algorithm co-optimization. *IEEE Transactions on Neural Networks and Learning Systems* 34, 10 (2022), 7660–7674.
- [14] Jimming Lu, Jiayi Tian, Hai Li, Ian Young, and Zheng Zhang. 2025. FETTA: Flexible and Efficient Hardware Accelerator for Tensorized Neural Network Training. *arXiv preprint arXiv:2504.06474* (2025).
- [15] Cheng Luo, Man-Kit Sit, Hongxiang Fan, Shuanglong Liu, Wayne Luk, and Ce Guo. 2020. Towards efficient deep neural network training by FPGA-based batch-level parallelism. *Journal of Semiconductors* 41, 2 (2020), 022403.
- [16] Alexander Novikov, Dmitrii Podoprikhin, Anton Osokin, and Dmitry P Vetrov. 2015. Tensorizing neural networks. *Advances in neural information processing systems* 28 (2015).
- [17] Ivan V Oseledets. 2011. Tensor-train decomposition. *SIAM Journal on Scientific Computing* 33, 5 (2011), 2295–2317.
- [18] Ritik Raj, Sarbartha Banerjee, Nikhil Chandra, Zishen Wan, Jianming Tong, Ananda Samajdar, and Tushar Krishna. 2025. SCALE-Sim v3: A modular cycle-accurate systolic accelerator simulator for end-to-end system analysis. In *2025 IEEE International Symposium on Performance Analysis of Systems and Software (ISPASS)*. IEEE, 186–200.
- [19] Yanan Sun, Bing Xue, Mengjie Zhang, and Gary G Yen. 2019. Evolving deep convolutional neural networks for image classification. *IEEE Transactions on Evolutionary Computation* 24, 2 (2019), 394–407.
- [20] Christian Szegedy, Alexander Toshev, and Dumitru Erhan. 2013. Deep neural networks for object detection. *Advances in neural information processing systems* 26 (2013).
- [21] Yue Tang, Xinyi Zhang, Peipei Zhou, and Jingtong Hu. 2022. EF-train: Enable efficient on-device CNN training on FPGA through data reshaping for online adaptation or personalization. *ACM Transactions on Design Automation of Electronic Systems (TODAES)* 27, 5 (2022), 1–36.
- [22] Jiayi Tian, Jimming Lu, Hai Li, Xiangwei Wang, Cong Callis Hao, Ian Young, and Zheng Zhang. 2025. Ultra Memory-Efficient On-FPGA Training of Transformers via Tensor-Compressed Optimization. *IEEE Transactions on Computer-Aided Design of Integrated Circuits and Systems* (2025).
- [23] Shreyas K Venkataramanaiah, Han-Sok Suh, Shihui Yin, Eriko Nurvitadhi, Aravind Dasu, Yu Cao, and Jae-sun Seo. 2020. FPGA-based low-batch training accelerator for modern CNNs featuring high bandwidth memory. In *Proceedings of the 39th International Conference on Computer-Aided Design*. 1–8.
- [24] Haonan Wang, Wenjian Liu, Tianyi Xu, Jun Lin, and Zhongfeng Wang. 2019. A low-latency sparse-winograd accelerator for convolutional neural networks. In *ICASSP 2019-2019 IEEE International Conference on Acoustics, Speech and Signal Processing (ICASSP)*. IEEE, 1448–1452.
- [25] Maolin Wang, Seyedramin Rasoulinezhad, Philip HW Leong, and Hayden K-H So. 2022. Niti: Training integer neural networks using integer-only arithmetic. *IEEE Transactions on Parallel and Distributed Systems* 33, 11 (2022), 3249–3261.
- [26] Qipeng Wang, Mengwei Xu, Chao Jin, Xinran Dong, Jinliang Yuan, Xin Jin, Gang Huang, Yunxin Liu, and Xuanzhe Liu. 2022. Melon: Breaking the memory wall for resource-efficient on-device machine learning. In *Proceedings of the 20th Annual International Conference on Mobile Systems, Applications and Services*. 450–463.
- [27] Daliang Xu, Mengwei Xu, Qipeng Wang, Shangguang Wang, Yun Ma, Kang Huang, Gang Huang, Xin Jin, and Xuanzhe Liu. 2022. Mandheling: Mixed-precision on-device dnn training with dsp offloading. In *Proceedings of the 28th Annual International Conference on Mobile Computing And Networking*. 214–227.
- [28] Zi Yang, Samridhi Choudhary, Siegfried Kunzmann, and Zheng Zhang. 2023. Quantization-aware and Tensor-compressed Training of Transformers for Natural Language Understanding. In *INTERSPEECH*.
- [29] Zi Yang, Ziyue Liu, Samridhi Choudhary, Xinfeng Xie, Cao Gao, Siegfried Kunzmann, and Zheng Zhang. 2024. Comera: Computing-and memory-efficient training via rank-adaptive tensor optimization. *Advances in Neural Information Processing Systems* 37 (2024), 77200–77225.
- [30] Miao Yin, Siyu Liao, Xiao-Yang Liu, Xiaodong Wang, and Bo Yuan. 2021. Towards extremely compact rnns for video recognition with fully decomposed hierarchical tucker structure. In *Proceedings of the IEEE/CVF Conference on Computer Vision and Pattern Recognition*. 12085–12094.
- [31] Miao Yin, Yang Sui, Siyu Liao, and Bo Yuan. 2021. Towards efficient tensor decomposition-based dnn model compression with optimization framework. In *Proceedings of the IEEE/CVF Conference on Computer Vision and Pattern Recognition*. 10674–10683.
- [32] Miao Yin, Yang Sui, Wanzhao Yang, Xiao Zang, Yu Gong, and Bo Yuan. 2022. Hodec: Towards efficient high-order decomposed convolutional neural networks. In *Proceedings of the IEEE/CVF Conference on Computer Vision and Pattern Recognition*. 12299–12308.
- [33] Jie-Fang Zhang, Cheng-Hsun Lu, and Zhengya Zhang. 2024. TetriX: Flexible architecture and optimal mapping for tensorized neural network processing. *IEEE Trans. Comput.* 73, 5 (2024), 1219–1232.